

RESEARCH ARTICLE | JUNE 26 2023

## Revisiting the Van Vleck second moment for characterizing molecular motion in organic solids

Special Collection: Modular and Interoperable Software for Chemical Physics

Simone Sturniolo  ; Helen M. Wickins  ; Paul Hodgkinson  

 Check for updates

*J. Chem. Phys.* 158, 244502 (2023)

<https://doi.org/10.1063/5.0151022>

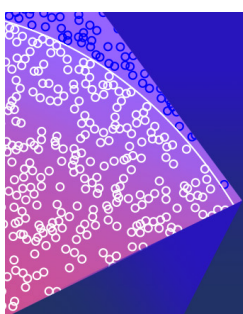


View  
Online



Export  
Citation

CrossMark



## The Journal of Chemical Physics

Special Topic: Monte Carlo methods,  
70 years after Metropolis *et al.* (1953)

**Submit Today**

 AIP  
Publishing

# Revisiting the Van Vleck second moment for characterizing molecular motion in organic solids

Cite as: J. Chem. Phys. 158, 244502 (2023); doi: 10.1063/5.0151022

Submitted: 17 March 2023 • Accepted: 7 June 2023 •

Published Online: 26 June 2023



View Online



Export Citation



CrossMark

Simone Sturniolo,<sup>1</sup> Helen M. Wickins,<sup>2</sup> and Paul Hodgkinson<sup>2,a)</sup>

## AFFILIATIONS

<sup>1</sup> Science and Technology Facilities Council, Rutherford Appleton Laboratory, Harwell Campus, Didcot OX11 0QX, United Kingdom

<sup>2</sup> Department of Chemistry, Durham University, Stockton Road, Durham DH1 3LE, United Kingdom

**Note:** This paper is part of the JCP Special Topic on Modular and Interoperable Software for Chemical Physics.

**a) Author to whom correspondence should be addressed:** paul.hodgkinson@durham.ac.uk

## ABSTRACT

Van Vleck's classic theory of the second moment of lineshapes in  $^1\text{H}$  nuclear magnetic resonance (NMR) is reworked in a form that allows the effect of rapid molecular motion on second moments to be calculated in a semi-analytical fashion. This is much more efficient than existing approaches and also extends previous analyses of (non-dynamic) dipolar networks in terms of site-specific root-sum-square dipolar couplings. The non-local nature of the second moment means that it can discriminate between overall motions that are difficult to discriminate using alternative approaches, such as measurements of NMR relaxation. The value of reviving second moment studies is illustrated on the plastic solids diamantane and triamantane. In the case of triamantane, straightforward measurements of  $^1\text{H}$  lineshapes on milligram samples show that the molecules in the higher temperature phase undergo multi-axis jumps, information that is not accessible either to diffraction studies or to alternative NMR approaches. The efficiency of the computational methods means that the second moments can be calculated using a readily extensible and open-source Python code.

© 2023 Author(s). All article content, except where otherwise noted, is licensed under a Creative Commons Attribution (CC BY) license (<http://creativecommons.org/licenses/by/4.0/>). <https://doi.org/10.1063/5.0151022>

## I. INTRODUCTION

The width of the  $^1\text{H}$  NMR spectrum is an easily measured and direct probe of molecular dynamics in organic materials. The spectra of dynamic solids show clear transitions from "static" lineshapes at low temperatures (when the dynamics are much slower than the width of the  $^1\text{H}$  spectrum) to narrower dynamically averaged spectra when the dynamics exceed the static linewidth (which is typically about 50 kHz). Calculating the spectral lineshape, however, requires diagonalization of the nuclear spin Hamiltonian, which rapidly becomes intractable for large numbers of dipolar-coupled spins. In contrast, Van Vleck demonstrated early in the development of NMR that the second moment of the NMR lineshape could be calculated analytically without diagonalization.<sup>1</sup>

Practical applications of the second moment require the calculation of the second moment in the presence of dynamics. This is straightforward for "intramolecular" contributions to the motion-

ally averaged second moment, that is, involving spin pairs that move together with the dynamic process.<sup>2</sup> There are, however, no general analytical expressions for the contribution of "intermolecular" dipolar couplings to the second moment.<sup>3</sup> Due to the slow convergence of sum over dipolar couplings with distance, the intermolecular and intramolecular contributions are typically similar in magnitude (see examples below), and so the intermolecular contribution cannot be neglected.

Second moments are generally evaluated in the high-field limit, i.e., the dipolar Hamiltonian is "truncated" to terms that commute with the dominant Zeeman interaction, introducing an orientation dependence to the second moment of solid samples. This dependence on the orientation of a crystallite with respect to the magnetic field axis is included analytically in the Van Vleck expressions derived for static samples. Existing approaches to calculating the intermolecular component of the second moment in the dynamic limit have, however, required a computationally

expensive numerical integration over a sphere in order to determine the orientationally averaged second moment. We provide below, however, analytical expressions that allow the second moment to be evaluated without such “powder averaging,” greatly reducing the computational burden. This allows the calculations to be performed in modern, portable programming languages rather than languages designed for computational efficiency. The only public code we have found for evaluating second moments is a Fortran-based code that is restricted to threefold diffusional rotation<sup>4</sup> and not applicable to the problem of interest. Given the complexity of calculating motionally averaged second moments, the lack of flexible public codes creates a significant hurdle to their practical use.

In this article, we make a case for reintroducing the <sup>1</sup>H second moment as a tool for probing dynamics in organic solids, especially in cases of whole molecular motion. In Sec. II, we re-present the theory of second moments in formulations that are more typical of modern treatments of NMR, in particular, making connections to “root-sum-square dipolar couplings,” which are a more straightforward, and easily understood, measure of the strength of dipolar coupling networks.<sup>5,6</sup> In Sec. III B, we present a Python code to evaluate second moments and evaluate the usefulness of second moments on a pair of soft solids from the diamondoid family of molecular organic solids.

## II. THEORY

### A. Second moment of static dipolar lineshapes

The spin Hamiltonian, in frequency units, of a set of dipolar-coupled nuclei is

$$\mathcal{H} = \mathcal{H}_Z + \mathcal{H}_D = \sum_j v_{j,\text{NMR}} \hat{S}_{jz} + \sum_{k>j} \hat{\mathbf{S}}_j \mathbf{D}_{jk} \hat{\mathbf{S}}_k, \quad (1)$$

where the first term is the Zeeman Hamiltonian and  $v_{j,\text{NMR}}$  is the Larmor frequency of spin  $j$  (potentially at this stage including the effects of chemical shifts). The second term corresponds to the dipolar couplings between spin pairs, with  $\hat{\mathbf{S}}$  representing the vector of spin operators ( $\hat{S}_x, \hat{S}_y, \hat{S}_z$ ). The dipolar coupling tensor,  $\mathbf{D}_{jk}$ , is axially symmetric (and traceless) and so can be described in terms of a single orientation vector,

$$\mathbf{D}_{jk} = D_{jk} (3\hat{\mathbf{r}}_{jk} \otimes \hat{\mathbf{r}}_{jk} - \mathbb{I}), \quad (2)$$

where  $\hat{\mathbf{r}}_{jk}$  is the unit vector between spins  $j$  and  $k$ ,  $\mathbb{I}$  is a  $3 \times 3$  identity matrix, and  $\otimes$  denotes the outer (or tensor) product of two vectors.  $D_{jk}$  is the dipolar coupling constant,

$$D_{jk} = -\frac{\mu_0 \hbar \gamma_j \gamma_k}{8\pi^2 r_{jk}^3}, \quad (3)$$

where the gyromagnetic ratios of the spins,  $\gamma_i$ , are expressed in rad s<sup>-1</sup> T<sup>-1</sup> and  $D_{jk}$  is expressed, as in Eq. (1), in frequency units.

In the high-field limit, the dipolar Hamiltonian for a set of like (homonuclear) spins is “truncated” to the normal expression

$$\mathcal{H}_{D,jk}^{\text{homo}} = D_{jk}^{\Omega} [3\hat{S}_{jz}\hat{S}_{kz} - \hat{\mathbf{S}}_j \hat{\mathbf{S}}_k] \quad D_{jk}^{\Omega} = D_{jk} \left( \frac{3\gamma_{jk}^2 - 1}{2} \right), \quad (4)$$

where superscript  $\Omega$  denotes a dipolar coupling constant which includes its dependence on crystallite orientation  $\Omega$ , and  $\gamma_{jk}$  is the

$zz$  direction cosine relating the direction of the internuclear vector,  $\hat{\mathbf{r}}_{jk} = (\alpha_{jk}, \beta_{jk}, \gamma_{jk})$ , to the magnetic field (conventionally oriented along  $z$ ).

Van Vleck’s key insight<sup>1</sup> was that diagonalization of the Hamiltonian is unnecessary if computing the second moment of the resulting spectral line. Provided we can neglect the effects on chemical shifts in comparison with dipolar couplings, which is an excellent approximation for wideline (static) <sup>1</sup>H NMR spectra, we can conveniently evaluate spectral moments in a frame rotating at the spectral midpoint,  $v_0$ , and the consequent symmetry about zero frequency means that it is sufficient to consider only the evolution of one, say  $x$ , component of the transverse ( $xy$ ) magnetization. In the Heisenberg formulation of quantum mechanics, the time dependence is put on the operator,

$$\frac{d\hat{F}_x}{dt} = i[\mathcal{H}_D, \hat{F}_x], \quad (5)$$

where  $\hat{F}_x = \sum_N \hat{S}_{xi}$  denotes the sum  $x$  operator over the  $N$  spins. Note that there are no factors involving  $h$ , since the Hamiltonian is expressed directly in frequency units. If we represent the operators as matrices and consider this equation element by element in a basis that diagonalizes the Hamiltonian with eigenvalues  $\varepsilon_n$ , then<sup>7,8</sup>

$$\frac{d(\hat{F}'_x)_{m,n}}{dt} = iv_{m,n}(\hat{F}'_x)_{m,n}, \quad (6)$$

i.e., the signal is a sum of oscillations at frequencies  $v_{m,n} = \varepsilon_m - \varepsilon_n$ . The amplitudes are given by  $A_{m,n} = |(\hat{F}'_x)_{m,n}|^2$ , where the ‘ indicates that the matrix elements are expressed in the basis that diagonalizes the Hamiltonian.

The normalized second moment of these oscillations, measured from an origin at  $v_0$ , is

$$\begin{aligned} M_2 &= \frac{\sum_{m,n} A_{m,n} v_{m,n}^2}{\sum_{m,n} A_{m,n}} \\ &= \frac{\sum_{mn} |(F'_x)_{mn}|^2 (\varepsilon_m - \varepsilon_n)^2}{\sum_{mn} |(F'_x)_{mn}|^2}. \end{aligned} \quad (7)$$

Note that  $M_2$  is expressed here in frequency units rather than the traditional definition in terms of angular frequency, which is denoted here as  $M_2^\omega$ , with  $M_2^\omega = 4\pi^2 M_2$ . Most literature values for <sup>1</sup>H second moments are reported in G<sup>2</sup> (reflecting acquisition using a varying magnetic field). These are related to the  $M_2$  above by

$$\begin{aligned} M_2 / \text{kHz}^2 &= 10^{-14} \left( \frac{\gamma_H}{2\pi} \right)^2 (M_2^\omega / \text{G}^2) \\ &= 18.128 (M_2^\omega / \text{G}^2) \end{aligned}$$

(using  $T \equiv 10^4$  G and  $\gamma_H = 2.6752 \times 10^8$  rad T<sup>-1</sup> s<sup>-1</sup>).

The key to evaluating Eq. (7) without diagonalization is reformulating the summations in terms of matrix traces using standard matrix algebra results,

$$\begin{aligned} \text{Tr}(|\mathbf{B}|^2) &= \sum_m (\mathbf{B}\mathbf{B}^\dagger)_{m,m} \\ &= \begin{cases} \sum_{m,n} |B_{m,n}|^2 & \text{if } \mathbf{B} \text{ is Hermitian,} \\ -\sum_{m,n} |B_{m,n}|^2 & \text{if } \mathbf{B} \text{ is anti-Hermitian.} \end{cases} \end{aligned} \quad (8)$$

Hence,

$$M_2 = -\frac{\text{Tr}([\mathcal{H}, \hat{F}_x'])^2}{\text{Tr}(\hat{F}_x'^2)}, \quad (9)$$

where the minus sign arises because the matrix with elements  $(\varepsilon_j - \varepsilon_k)(F'_x)_{jk}$  is anti-Hermitian. Since Eq. (9) only features traces of matrices, it is valid in any eigenbasis, including the much more convenient eigenbasis of the Zeeman Hamiltonian, which allows the ' $\prime$ ' to be dropped. Evaluating the commutator in the numerator for the Hamiltonian of Eq. (4) is then straightforward from the properties of angular momentum operators,

$$[\hat{S}_j \hat{S}_k, \hat{F}_x] = 0, \quad (10)$$

$$[\hat{S}_{jz} \hat{S}_{kz}, \hat{F}_x] = i(\hat{S}_{jy} \hat{S}_{kz} + \hat{S}_{jz} \hat{S}_{ky}). \quad (11)$$

Again, the commutators do not contain factors of  $\hbar$  since these are operators returning frequencies rather than true angular momentum operators. Hence,

$$[\mathcal{H}_D^{\text{homo}}, \hat{F}_x] = 3i \sum_{k>j} D_{jk}^\Omega (\hat{S}_{jy} \hat{S}_{kz} + \hat{S}_{jz} \hat{S}_{ky}). \quad (12)$$

The traces of squared spin operators are independent of axis labeling and easily evaluated for  $z$  in the Zeeman basis. Similarly, traces involving different spins can be evaluated in  $z$  for the two spins independently, e.g.,

$$\text{Tr}(\hat{S}_{1x} \hat{S}_{2y}) = \text{Tr}(\hat{S}_{1z} \hat{S}_{2z}) = 0.$$

Hence, for a system of  $N$  spins of the quantum number  $S$ , the following relationships hold:<sup>1</sup>

$$\text{Tr}(\hat{S}_{ja}^2) = \frac{1}{3} S(S+1)(2S+1)^N, \quad (13)$$

$$\text{Tr}(\hat{S}_{ja} \hat{S}_{kb}) = \text{Tr}(\hat{S}_{ja}^2 \hat{S}_{kb}^2) = 0 \quad \text{for } j \neq k \text{ and any } a, b \text{ in } \{x, y, z\}, \quad (14)$$

$$\text{Tr}(\hat{S}_{ja}^2 \hat{S}_{kb}^2) = \frac{1}{9} S^2 (S+1)^2 (2S+1)^N \quad \text{for any } a, b \text{ in } \{x, y, z\}. \quad (15)$$

Combining Eqs. (14) and (15) with Eq. (12),

$$\text{Tr}([\mathcal{H}_D^{\text{homo}}, \hat{F}_x]^2) = -9 \times \frac{2}{9} S^2 (S+1)^2 (2S+1)^N \sum_{k>j} (D_{jk}^\Omega)^2, \quad (16)$$

where the factor of two arises from the two pairs of terms of the form  $\hat{S}_{ja}^2 \hat{S}_{kb}^2$  from squaring Eq. (12). From Eqs. (13) and (14), the other trace evaluates to

$$\text{Tr}(\hat{F}_x'^2) = \frac{N}{3} S(S+1)(2S+1)^N, \quad (17)$$

since there are  $N$  terms of the form  $\text{Tr}(\hat{S}_{ja}^2)$  and the “cross-terms” are zero. Hence, we obtain

$$M_2^{\text{homo},\Omega} = \frac{6}{N} S(S+1) \sum_{k>j} (D_{jk}^\Omega)^2, \quad (18)$$

where the  $\Omega$  superscript indicates that its value will depend on crystallite orientation  $\Omega$ .

Re-writing the double sum to give equal treatment to all spins,

$$M_2^{\text{homo},\Omega} = \frac{3}{N} S(S+1) \sum_k \sum_{j \neq k} (D_{jk}^\Omega)^2. \quad (19)$$

In practice, we need to determine the second moment averaged over crystallite orientations. The orientationally averaged  $(D_{jk}^\Omega)^2$  terms are

$$\langle (D_{jk}^\Omega)^2 \rangle_\Omega = D_{jk}^2 \langle [P_2(\cos \theta)]^2 \rangle_\Omega = \frac{1}{5} D_{jk}^2, \quad (20)$$

where  $\langle \rangle_\Omega$  denotes the average over the orientation  $\Omega$  (expressed in terms of the two spherical angles), and using

$$\langle [P_2(\cos \theta)]^2 \rangle_\Omega = \frac{\int^\Omega [P_2(\cos \theta)]^2 d\Omega}{\int^\Omega d\Omega} = \frac{1}{5}. \quad (21)$$

Hence, the orientationally averaged second moment is

$$M_2 = \langle M_2^{\text{homo},\Omega} \rangle_\Omega = \frac{3}{5} S(S+1) \langle D_{k,\text{rss}}^2 \rangle_N \quad (22)$$

$$= \frac{9}{20} \langle D_{k,\text{rss}}^2 \rangle_N \quad \text{for } S = 1/2, \quad (23)$$

where  $\langle \rangle_N$  denotes the average over the spins, and  $D_{k,\text{rss}}$  is the root-sum-square (RSS) coupling for site  $k$ ,

$$D_{k,\text{rss}} = \sqrt{\sum_{j \neq k} (D_{jk})^2}. \quad (24)$$

The RSS coupling has proved a useful and intuitive metric for the strength of the local dipolar coupling network.<sup>5,6</sup> This formulation of the second moment also avoids the assumption, made in classic derivations, that the spins are somehow “equivalent”; within the approximation that dipolar couplings dominate the lineshape, these expressions are exact, even if different sites have different dipolar environments. As noted for diamantane in the sample output in the supplementary material, there can be significant variations between the  $D_{\text{rss}}$  values for different H environments.

## B. Rotating molecules

Formally, the second moment is invariant to motion. As discussed by Abragam,<sup>3</sup> however, the *observable* second moment is reduced by fast dynamics and is determined by the time-averaged Hamiltonian (as is assumed without comment in most literature on second moments). Splitting the Hamiltonian into time-dependent and time-independent terms, the key trace in Eq. (9) becomes

$$\text{Tr}([\mathcal{H}(t), \hat{F}_x]^2) = \text{Tr}([\langle \mathcal{H} \rangle, \hat{F}_x]^2) + \langle [\mathcal{H}(t) - \langle \mathcal{H} \rangle, \hat{F}_x]^2 \rangle, \quad (25)$$

where  $\langle \rangle$  refers to averaging over time,  $t$ . The first-term determines the observable second moment and corresponds to evaluating the second moment with the time-averaged dipolar Hamiltonian. The associated lineshape will have a strong Gaussian character, which is practically significant, as noted below. In contrast, the second term will involve frequencies over a wide frequency range (determined by the characteristic frequency of the motion). In the limit of fast motion being considered, these will be outside the spectral width.<sup>3</sup> Hence, although mathematically significant for preserving the invariance of the second moment, the second term is effectively unobservable.

For systems with long-range order, we can, in principle, use second moments quantitatively to distinguish between different dynamic processes. As noted above, however, there are no general analytical expressions for evaluating the intermolecular component of the second moment in the presence of dynamics. Moreover, the classic Van Vleck expressions, re-derived above, assume “normal” dipolar tensors with zero asymmetry. Since dynamic averaging can result in average tensors with a non-zero asymmetry parameter (typically from averaging over two-site jumps), the above-mentioned standard expressions cannot be used.

We can, however, straightforwardly extend the above-mentioned derivation to calculate second moments directly from the principal values of dynamically averaged tensors,  $\bar{\mathbf{D}}_{jk}$ . For a conventional dipolar coupling tensor, the  $zz$  term in the high-field limit is  $(\mathbf{D}_{jk}^L)_{zz} = 2D_{jk}^\Omega$ , where L denotes the laboratory frame and  $D_{jk}^\Omega$  depends (only) on the  $\theta$  spherical angle as in Eq. (4). By analogy with the quadrupolar coupling tensor,<sup>9</sup> the corresponding term of a general average dipolar coupling tensor will depend on both  $\theta$  and  $\phi$  polar angles as

$$(\bar{\mathbf{D}}_{jk}^L)_{zz} = 2D_{jk}\left(\frac{3\cos^2\theta - 1}{2} + \eta\sin^2\theta\cos 2\phi\right). \quad (26)$$

Note that the sign of the  $\eta$  term will depend on the conventions used for ordering axes and defining the  $\phi$  polar angle, but is irrelevant for the final result.

The individual (orientationally averaged) contributions to the sum-square couplings are given by

$$\langle (D_{jk}^\Omega)^2 \rangle_\Omega = D_{jk}^2\left(\frac{1}{5} + \frac{\eta^2}{15}\right), \quad (27)$$

where the following orientational averages have been used [in addition to Eq. (21)]:

$$\langle (3\cos^2\theta - 1)\sin^2\theta\cos 2\phi \rangle_\Omega = 0, \quad (28)$$

$$\langle \sin^4\theta\cos^2 2\phi \rangle_\Omega = \frac{1}{15}. \quad (29)$$

This minor modification to Eq. (20) effectively extends to the applications of root-sum-square couplings to any system where tensors have been averaged by fast dynamics. It also allows orientationally averaged second moments to be efficiently calculated using the existing relationship between  $M_2$  and  $D_{k,\text{rss}}$  values [Eq. (23)].

The “intermediate” timescale, in which the motional correlation time lies between the limits of fast and slow motion, is

considerably more complex and is not discussed here; see Ref. 10 and references therein. It is worth noting, however, that a pre-condition for analyzing the intermediate regime is that the fast-motion limit of  $M_2$  is known,<sup>11</sup> either from experiment or from calculation.

### III. COMPARISON WITH EXPERIMENT

#### A. Experimental details

Experimental  $^1\text{H}$  NMR data were acquired as a part of a wider study of dynamics in diamondoid materials. Experimental details and raw data are provided for the subset of results used here for experimental verification.

To maintain sample history across static and spinning experiments, samples were packed into 4 mm zirconia rotors, which were placed in a 5 mm glass holder to ensure that the filled rotor was in the center of the coil. In contrast to diamantane, which is available commercially, there was limited triamantane sample available ( $\sim 20$  mg). Hence, the limited volume of sample was sealed inside a Kel-F (polychlorotrifluoroethylene) insert before packing into the zirconia rotor. Static wideline solid-state NMR  $^1\text{H}$  spectra were obtained using a Bruker Avance III HD spectrometer operating at 400.17 MHz and a static 5 mm probe. Spectra were recorded using a solid echo (SE) with a 15  $\mu\text{s}$  inter-pulse echo delay. The triamantane spectra below 469 K showed significant signal from the Kel-F insert, and so additional spectra (denoted IR) were acquired using inversion recovery with a delay between 0.5 and 1.0 s to approximately nullify this more rapidly relaxing component.

Three different sample temperatures were analyzed for each material: 211, 411, and 498 K for diamantane, corresponding to three distinct motional regimes observed in earlier studies, and 192, 360, and 469 K for triamantane, corresponding to the static limit and two distinct motional regimes (see Figs S5 and S6 in the supplementary material for plots of the temperature dependence of  $M_2$ ). In both cases, the highest temperature corresponds to a highly dynamic regime in which bulk molecular diffusion is likely to be present (by analogy with the behavior of adamantane<sup>12</sup>). Note that the static limit for diamantane (transition temperature 135 K<sup>13</sup>) could not be accessed using the equipment available. Temperatures were calibrated using ethylene glycol and methanol (details in the data archive), with an estimated uncertainty on individual presented temperatures of  $\pm 5$  K.

#### B. Calculation implementation

The calculation of second moments in crystalline systems was implemented in Python 3 using the Soprano library for NMR crystallography, which in turn relies on the Atomic Simulation Environment (ASE) library,<sup>14</sup> a widely used support library for atomistic calculations. The unit cell of the starting structure can then be specified using any format read by ASE (although typically CIF) and is assumed to be a three-dimensional periodic structure of a molecular solid. The distinct molecules in the unit cell are identified by Soprano functions on the basis of short internuclear distances (compared to the sum of Van der Waals radii). The use of standardized libraries allows the code to be kept compact and readily extensible, in contrast to previous monolithic codes. In its current form, vanVleck Calculator assumes that the motion involves whole molecules undergoing  $n$ -fold diffusional rotation about one or more

axes. These axes are specified in terms of site labels present in the initial structure, for instance, the  $C_2$  axis in diamantane links carbon atoms with labels C1 and C53. The effects of combined  $n$ - and  $m$ -fold rotations on the atomic positions are evaluated to produce an  $M = n \times m \times \dots$  set of atomic positions.

The effects of dynamics on intermolecular couplings cannot be expressed analytically since the magnitude and orientation of the dipolar tensors change as the spins move relative to each other. It is straightforward, however, to numerically average tensors over the motion. The intramolecular contributions to the second moment are evaluated for a “reference” molecule containing the rotation axis/axes, and the dipolar tensors are averaged over the  $M$  molecular positions. For intermolecular couplings, and assuming the same uncorrelated motion on all molecules, there will be  $M^2$  pairs of relative molecular orientations,

$$\langle \mathbf{D}_{jk}^{\text{inter}} \rangle = \frac{1}{M^2} \sum_l^M \sum_m^M \mathbf{D}_{jk}(\Phi_l, \Phi_m), \quad (30)$$

in which each tensor is computed using the internuclear vectors  $\mathbf{r}_{jk}(\Phi_l, \Phi_m)$  corresponding to the different orientational states,  $\Phi$ , of the two molecules. The averaged tensors will not, in general, have axial symmetry ( $\eta = 0$ ), and so the Van Vleck formulae cannot be used. The solution in the previous literature, e.g., Ref. 15, was to compute second moments from explicit calculations of motionally averaged  $D_{jk}^\Omega$  terms. Because these values depend on the crystallite orientation, a computationally expensive powder average is needed.<sup>16</sup> In contrast, here we use Eq. (27) to calculate  $M_2$  values directly from the eigenvalues of the averaged tensors obtained from Eq. (30), considerably improving computational efficiency. The overall efficiency means that there is little benefit in removing symmetry-equivalent combinations of  $\Phi_l, \Phi_m$ .

The total intermolecular and intramolecular contributions to the sum-square coupling are evaluated for each H site of the reference molecule. The intermolecular component of the second moment converges relatively slowly with increasing distance. The cut-off is specified in terms of a radius from the center of mass of the “reference” molecule; only “remote” molecules with a center of mass within the radius are included in the summation. Finally, the overall second moment is determined from the mean of the sum-square couplings at each site [Eq. (23)]. A sample output is given in Sec. III of the supplementary material.

### C. Discussion

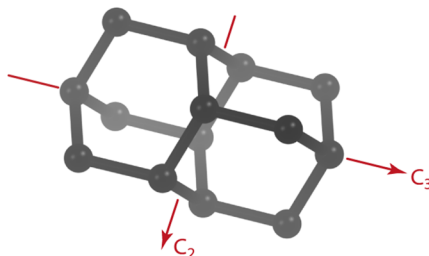
Table I shows the results of calculating second moments on diamantane and triamantane using the approach described above and different models for the motion shown in Fig. 1. Including molecules up to a radius of 20 Å from the reference molecule (which corresponded to 134 and 108 molecules for diamantane and triamantane, respectively) provided values that converged to 0.1 kHz<sup>2</sup>. The crystal structures were taken from the Cambridge structural database<sup>17</sup> (refcodes CONGRS and TRIAMT01 for diamantane and triamantane, respectively). As noted in a previous study to calculate  $D_{\text{rss}}$  values from crystal structures,<sup>5</sup> using uncorrected H positions can lead to unreliable results; e.g., the calculated dipolar coupling within a CH<sub>2</sub> is extremely sensitive to systematic errors in C–H distances in the associated x-ray diffraction studies. Hence, the H positions were relaxed using CASTEP<sup>18</sup> (at fixed unit cell geometry). In the case of

**TABLE I.** Calculated powder-averaged  $M_2$  values (in kHz<sup>2</sup>) for different motional models.

	Intramolecular	Intermolecular	Total
<b>Diamantane</b>			
Static	261.3	138.2	399.5
$C_2$	164.2	43.3	207.4
$C_3$	67.0	35.4	102.4
$C_3 + C_2$	67.0	16.4	83.5
<b>Triamantane</b>			
Static	260.7	128.7	389.4
$C_2$	147.9	42.0	189.9
Pseudo- $C_2$ (long)	165.7	46.6	212.3
Pseudo- $C_2$ (short)	173.3	43.8	217.1
Any two $C_2$ -like axes	113.1	18.7	131.8

diamantane, for example, the second moment was over-estimated by about 15% using un-optimized diffraction co-ordinates. In contrast, there was a negligible difference in calculated  $M_2$  values depending on whether just H positions or all atomic positions were relaxed. Note how the intermolecular contribution to the second moment is not negligible, especially in the static limit, but even in the dynamic

### Diamantane



### Triamantane

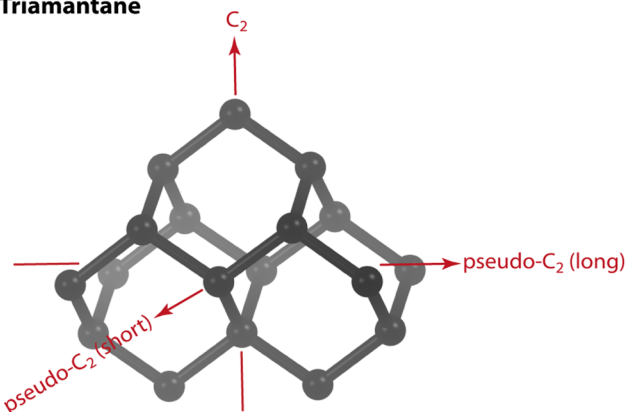


**FIG. 1.** Molecular structures of diamantane and triamantane, illustrating motional axes considered in the second moment analysis.

case, neglecting that intermolecular component would lead to significant discrepancies with experimental values. Historically, this has complicated the practical application of second moments; in the earlier study of diamantane motion via second moments,<sup>13</sup> the intermolecular contribution was estimated in a rather ad hoc way by analogy with similar systems.

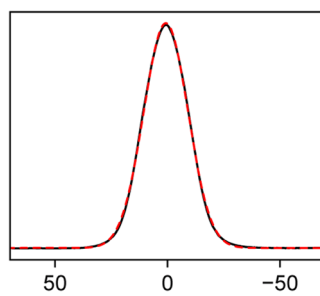
Considering the values in Table I, it is unsurprising that rotation about a  $C_n$  axis with  $n > 2$  (diamantane) leads to a very large reduction in second moment, which is measurably different from the effects of twofold rotations. Note how the introduction of a  $C_2$  motion has no effect on the intramolecular component of  $M_2$ , since the dipolar tensors averaged by the  $C_3$  motion are invariant to a  $C_2$  around a perpendicular axis. In the case of triamantane, three  $C_2$ -like motions can be proposed. Note that any pair of  $C_2$ -like motions generates the third, and so there is no physical significance to considering all three motions simultaneously, and the same value of  $M_2$  is obtained for any pair of the  $C_2$ -like motions. The second moment values, however, differ measurably between models involving a single  $C_2$ -like motion and two such motions.

Various approaches were evaluated to determine the second moment from the experimental data. As discussed in the supplementary material, it was difficult to obtain consistent values for the second moment in the static limit, i.e., triamantane at 192 K, and these tended to over-estimate  $M_2$  compared to calculations. These discrepancies are thought to arise from contributions of higher-order moments when using spin-echoes for detection.<sup>19</sup> On the other hand, the lineshapes in the “intermediate” temperature regime have a strong Gaussian character, and robust and consistent values could be obtained. In the high temperature limit, where  $M_2$  is small, the lineshape is increasingly determined by relaxation and develops Lorentzian characteristics. Second-moment analysis is, therefore, inappropriate in this limit.

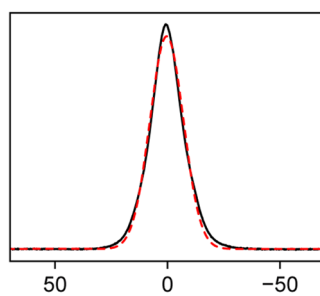
Figure 2 shows the quantification of the experimental second moment of the diamantane and triamantane samples in the key “intermediate” regime in which the  $^1\text{H}$  lineshape is partially averaged by dynamics. In agreement with the predictions noted previously,<sup>3</sup> the spectra in this regime fit well to Gaussian functions; similar observations have been made for dipolar lineshapes averaged by magic-angle spinning.<sup>20</sup> The experimental values shown in Table II are quoted to the nearest 5 kHz<sup>2</sup>. This estimated uncertainty is much larger than the very small statistical uncertainties in the fitting (shown in Table S1 in the supplementary material), which simply reflect the high signal-to-noise ratio of the  $^1\text{H}$  spectra. This 5 kHz<sup>2</sup> figure is a more reasonable estimate of the uncertainty in the experimental values; as shown in Figs S5 and S6 of the supplementary material, the second moment values steadily increase with temperature as a result of increased molecular libration, introducing significant uncertainty in estimating a second moment free of librational effects.

As shown in Table II, the motion of diamantane at 221 K is clearly consistent with rapid dynamics about its  $C_3$  symmetry axis. The dynamics in the higher temperature regime (sampled here at 441 K) indicates that the molecules are constrained but are undergoing significantly more motion than at 221 K. This motion has previously been described in terms of rotation about an additional “L” axis tilted away from the symmetry axis.<sup>13</sup> A more likely scenario is that there is significant overall motion of molecules at these elevated temperatures, permitting frequent flips around their  $C_2$  axes

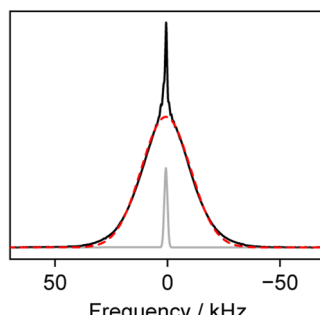
Diamantane, 221 K



Diamantane, 411 K



Triamantane, 360 K



Frequency / kHz

FIG. 2. Static  $^1\text{H}$  spectra (solid black) fitted to Gaussian lineshapes (dashed red), including, if needed, an additional Gaussian (gray) to fit out the insert signal. The fitted  $M_2$  values are shown in Table II.

(corresponding to a jump-only value of  $M_2$  of 83.5 kHz<sup>2</sup>), plus a significant reduction of  $M_2$  due to the overall motion and associated thermal expansion of the lattice (cf. the temperature of  $M_2$  in Fig. S5).

In the case of triamantane, the second-moment results clearly show that the dynamics of the molecules must involve jumps about multiple  $C_2$ -like axes. The energetic barriers are expected to be lowest for the symmetry-preserving  $C_2$  and the symmetry-breaking “top over bottom” flip of the molecule about the long molecular axes. As in the case of diamantane, the experimental second moment in the high temperature regime is significantly smaller than the prediction from an idealized motion, due to overall libration. This picture is consistent with diffraction data in which a gradual order-disorder transition between 273 and 303 K was found to be associated with

**TABLE II.** Experimental  $M_2$  values (to the nearest 5 kHz $^2$ ) and best match from calculated values.

Experiment	Calculated
<b>Diamantane</b>	
221 K	100
411 K	55
<b>Triamantane</b>	
360 K	120
Two C <sub>2</sub> axes: 131.8	

an additional pseudo-mirror plane corresponding to a symmetry-breaking flip of the molecules.<sup>21</sup> Crucially, however, the diffraction data are not sensitive to the symmetry-preserving C<sub>2</sub> motion and so the NMR data, via the second moments, are providing a more complete picture of the dynamics in this material.

It is important to note that attempts to understand the motion of triamantane by other techniques were unsuccessful; indeed, this provided the initial motivation to consider using <sup>1</sup>H second moments. In particular, it was not possible to distinguish between motional models for triamantane using <sup>13</sup>C relaxation time measurements. First, because there was a narrow window between phase transition temperatures and the point at which <sup>13</sup>C linewidths were too degraded by interference between the dynamics and the <sup>1</sup>H decoupling.<sup>22</sup> Second, and in contrast to diamantane, in which the C<sub>3</sub> motion has a distinctly different effect on different C–H bond vectors, the C<sub>2</sub>-like motions in triamantane all have similar effects on individual bond vectors. Hence, it was not possible to identify the motion using <sup>13</sup>C relaxation time constants calculated for specific motional models.<sup>23</sup> In contrast, the second moment contains a significant “non-local” contribution, via the intermolecular component. Relaxation times, for either <sup>13</sup>C or <sup>1</sup>H, also struggle to distinguish between large and small amplitude motions; in particular, a large amplitude motion that leads to an inversion of the NMR tensor will not modulate the interaction and will not affect relaxation times. This inherent ambiguity is much less likely in second-moment values since they are summed over multiple dipolar interactions, which are affected both by orientation with respect to the external field and by the physical distances between atoms. On the other hand, the differences in averaged second moment between alternative C<sub>2</sub>-like axes in Table I are generally small, i.e., it is not realistic to distinguish between very similar motional models using second-moment data.

As recently argued in the context of polymeric materials,<sup>10</sup> we argue that the <sup>1</sup>H second moment is a useful complementary tool for studying molecular reorientation in organic solids. Extending Van Vleck’s original derivation, we can efficiently calculate site-resolved root-sum-square couplings and second moments for different motional models in crystalline materials. The code is publicly available<sup>24</sup> and can be readily modified to include more complex scenarios than the plastic crystalline materials considered here.

## SUPPLEMENTARY MATERIAL

The supplementary material contains a discussion of different methods for quantifying the experimental second moment, the full temperature dependence of  $M_2$  for diamantane and triamantane, and a sample output from the calculation.

## ACKNOWLEDGMENTS

We are indebted to Professor Robert Glaser for providing the samples of the diamondoid materials studied. P.H. and H.M.W. acknowledge the Leverhulme Trust for providing financial support (Grant No. RPG-2018-288). This work was facilitated by software tools (specifically Soprano) developed by S.S. through the Collaborative Computing Project for NMR Crystallography (EPSRC Grant No. EP/T026642/1).

## AUTHOR DECLARATIONS

### Conflict of Interest

The authors have no conflicts to disclose.

### Author Contributions

**Simone Sturniolo:** Software (lead); Writing – original draft (lead). **Helen M. Wickins:** Data curation (lead); Investigation (lead); Writing – review & editing (supporting). **Paul Hodgkinson:** Funding acquisition (lead); Software (supporting); Supervision (lead); Writing – review & editing (lead).

## DATA AVAILABILITY

The data that support the findings of this study are openly available at <http://doi.org/10.15128/r1qz20ss572>. The code developed is publicly available.<sup>24</sup>

## REFERENCES

1. J. H. Van Vleck, “The dipolar broadening of magnetic resonance lines in crystals,” *Phys. Rev.* **74**, 1168 (1948).
2. H. S. Gutowsky and G. E. Pake, “Structural investigations by means of nuclear magnetism. II. Hindered rotation in solids,” *J. Chem. Phys.* **18**, 162 (1950).
3. A. Abragam, *Principles of Nuclear Magnetism* (Oxford University Press, 1961), Chap. X, pp. 424–479.
4. R. Goc, “Computer calculation of the Van Vleck second moment for materials with internal rotation of spin groups,” *Comput. Phys. Commun.* **162**, 102 (2004).
5. V. E. Zorin, S. P. Brown, and P. Hodgkinson, “Origins of linewidth in <sup>1</sup>H magic-angle spinning NMR,” *J. Chem. Phys.* **125**, 144508 (2006).
6. V. E. Zorin, S. P. Brown, and P. Hodgkinson, “Quantification of homonuclear dipolar coupling networks from magic-angle spinning <sup>1</sup>H NMR,” *Mol. Phys.* **104**, 293 (2006).
7. P. Hodgkinson and L. Emsley, “Numerical simulation of solid-state NMR experiments,” *Prog. Nucl. Magn. Reson. Spectrosc.* **36**, 201 (2000).
8. M. Edén, “Computer simulations in solid-state NMR. I. Spin dynamics theory,” *Concepts Magn. Reson.* **17A**, 117 (2003).
9. D. C. Apperley, R. K. Harris, and P. Hodgkinson, *Solid-State NMR Basic Principles and Practice* (Momentum Press, New York, 2012).

- <sup>10</sup>T. M. Alam, J. P. Allers, and B. H. Jones, "Heterogeneous polymer dynamics explored using static <sup>1</sup>H NMR spectra," *Int. J. Mol. Sci.* **21**, 1 (2020).
- <sup>11</sup>P. Bilski, M. Olszewski, N. A. Sergeev, and J. Waśicki, "Calculation of dipolar correlation function in solids with internal mobility," *Solid State Nucl. Magn. Reson.* **25**, 15 (2004).
- <sup>12</sup>H. A. Resing, N. T. Corke, and J. N. Sherwood, "Self-diffusion in the molecular crystal adamantane; comparison of NMR and plastic-flow methods," *Phys. Rev. Lett.* **20**, 1227 (1968).
- <sup>13</sup>A. R. Britcher and J. H. Strange, "Molecular motion in solid diamantane studied by nuclear magnetic resonance," *J. Chem. Soc. Faraday Trans. 2* **74**, 1767 (1978).
- <sup>14</sup>A. H. Larsen, J. J. Mortensen, J. Blomqvist, I. E. Castelli, R. Christensen, M. Dušák, J. Friis, M. N. Groves, B. Hammer, C. Hargus, E. D. Hermes, P. C. Jennings, P. B. Jensen, J. Kermode, J. R. Kitchin, E. L. Kolsbjerg, J. Kubal, K. Kaasbjerg, S. Lysgaard, J. B. Maronsson, T. Maxson, T. Olsen, L. Pastewka, A. Peterson, C. Rosgaard, J. Schiotz, O. Schütt, M. Strange, K. S. Thygesen, T. Vegge, L. Vilhelmsen, M. Walter, Z. Zeng, and K. W. Jacobsen, "The atomic simulation environment—A Python library for working with atoms," *J. Phys.: Condens. Matter.* **29**, 273002 (2017).
- <sup>15</sup>R. Goc, "Calculation of the NMR second moment for materials with different types of internal rotation," *Solid State Nucl. Magn. Reson.* **13**, 55 (1998).
- <sup>16</sup>R. Goc, "Effective spatial averaging for NMR second moment calculation," *J. Magn. Reson.* **132**, 78 (1998).
- <sup>17</sup>C. R. Groom, I. J. Bruno, M. P. Lightfoot, and S. C. Ward, "The Cambridge structural database," *Acta Cryst. B* **72**, 171 (2016).
- <sup>18</sup>S. J. Clark, M. D. Segall, C. J. Pickard, P. J. Hasnip, M. I. J. Probert, K. Refson, and M. C. Payne, "First principles methods using CASTEP," *Z. Krist.-Cryst. Mater.* **220**, 567 (2005).
- <sup>19</sup>P. K. Kahol, "Evaluation of moments from the NMR solid echoes in dipolar solids," *Phys. Status Solidi B* **159**, 873 (1990).
- <sup>20</sup>A. A. Malär, S. Smith-Penzel, G.-M. Camenisch, T. Wiegand, A. Samoson, A. Böckmann, M. Ernst, and B. H. Meier, "Quantifying proton NMR coherent linewidth in proteins under fast MAS conditions: A second moment approach," *Phys. Chem. Chem. Phys.* **21**, 18850 (2019).
- <sup>21</sup>R. Cernik, E. H. M. Evans, R. Hine, and J. P. G. Richards, "Phase transitions in triamantane," *Solid State Commun.* **27**, 1017 (1978).
- <sup>22</sup>W. P. Rothwell and J. S. Waugh, "Transverse relaxation of dipolar coupled spin systems under RF irradiation: Detecting motions in solids," *J. Chem. Phys.* **74**, 2721 (1981).
- <sup>23</sup>D. C. Apperley, A. F. Markwell, I. Frantsuzov, A. J. Ilott, R. K. Harris, and P. Hodgkinson, "NMR characterisation of dynamics in solvates and desolvates of formoterol fumarate," *Phys. Chem. Chem. Phys.* **15**, 6422 (2013).
- <sup>24</sup>See [https://github.com/CCP-NC/dipolar\\_averages](https://github.com/CCP-NC/dipolar_averages) for dipolar\_averages (last accessed June 2023).